Nanoscale Advances

ROYAL SOCIETY OF CHEMISTRY

PAPER

View Article Online
View Journal | View Issue

Cite this: *Nanoscale Adv.*, 2024, **6**, 4426

Nanocomposites based on Cu_2O coated silver nanowire networks for high-performance oxygen evolution reaction†

Sergio Battiato, [ab] Abderrahime Sekkat,[cd] Camilo Sanchez Velasquez,[c] Anna Lucia Pellegrino,[e] Daniel Bellet, [c] Antonio Terrasi,[ab] Salvo Mirabella[ab] and David Muñoz-Rojas *[c]

Received 2nd May 2024
Accepted 26th June 2024

DOI: 10.1039/d4na00364k

rsc.li/nanoscale-advances

The development of highly active, low-cost, and robust electrocatalysts for the oxygen evolution reaction (OER) is a crucial endeavor for the clean and economically viable production of hydrogen *via* electrochemical water splitting. Herein, cuprous oxide (Cu_2O) thin films are deposited on silver nanowire (AgNW) networks by atmospheric-pressure spatial atomic layer deposition (AP-SALD). AgNW@Cu_2O nanocomposites supported on conductive copper electrodes exhibited superior OER activity as compared to bare copper substrate and bare AgNWs. Moreover, a relationship between Cu_2O thickness and OER activity was established. Notably, the most effective catalyst (AgNW@50nm-thick Cu_2O) demonstrated very high OER activity with a low overpotential of 409 mV to deliver a current density of 10 mA cm^{-2} (η_{10}), a Tafel slope of 47 mV dec^{-1}, a turnover frequency (TOF) of 4.2 s^{-1} at 350 mV, and good durability in alkaline media (1 M KOH). This highlights the potential of AgNWs as a powerful platform for the formation of highly efficient copper oxide catalysts towards OER. This work provides a foundation for the development of nanostructured Cu-based electrocatalysts for future clean energy conversion and storage systems.

1. Introduction

The ever-increasing global energy demand and severe environmental concerns have strengthened focus on developing brand-new clean and renewable energy sources.[1,2] In this context, green hydrogen produced from electrochemical water splitting is expected to be a major contender for future energy conversion technologies.[3,4] Despite its huge potential to meet clean energy requirements, widespread adoption of water splitting technology is severely hampered by the thermodynamic uphill oxygen evolution reaction (OER), involving several proton and electron transfer steps with a high Gibbs free energy, resulting in high overpotentials that drive the overall process.[5–8] Therefore, the deployment of water electrolysis as a viable process for clean hydrogen production largely hinges on the development of efficient and inexpensive OER catalysts.[9,10] Over the past few years, many compounds have been proposed as OER electrode materials, particularly transition metal-based electrocatalysts, such as oxides,[11–13] phosphides,[14,15] and sulfides,[16] among others. Among them, Cu-based materials emerge as compelling candidates on account of their cost, earth-abundance of Cu, and non-toxicity.[17,18] Despite all these advantages, very few studies have focused their attention on this class of materials towards OER targeted applications. For instance, Chun-Chao Hou *et al.*, have reported Cu-based nanowire arrays targeted for OER application that showed η_{10} about 530 mV, remaining stable for at least 7 h.[19] Similarly, Yu *et al.* have recently reported Cu_xO layers for OER catalysis with $\eta_{10} = 500$ mV, which worked at a steady state value for at least 15 h.[20] Even though the Cu-based electrodes in the above-mentioned works were found to show appreciable OER performance, their activity and stability are unsatisfactory when compared to the benchmark OER electrocatalysts (*i.e.*, IrO_x and RuO_x).[21,22] Hence, the development of Cu-based electrocatalysts with high catalytic activity and stability remains a challenge. This is aligned with the development of conducting supports such as a Ag framework that increases the surface-active sites, which can be synthesized with scalable processes such as spray coating,[23] chemical vapor deposition,[24] and solution-phase approaches,[25] among others that result in catalysts with very high OER activities and stabilities.[26]

[a]*Dipartimento di Fisica e Astronomia "Ettore Majorana", Università di Catania, Via Santa Sofia 64, 95123 Catania, Italy*
[b]*CNR-IMM, Via Santa Sofia 64, 95123 Catania, Italy*
[c]*Univ. Grenoble Alpes, CNRS, Grenoble INP, LMGP, Grenoble, France. E-mail: david.munoz-rojas@grenoble-inp.fr*
[d]*Laboratoire de Génie Chimique, Université de Toulouse, CNRS, Toulouse, France*
[e]*Dipartimento di Scienze Chimiche, Università di Catania, INSTM UdR Catania, Viale Andrea Doria 6, I-95125 Catania, Italy*

† Electronic supplementary information (ESI) available. See DOI: https://doi.org/10.1039/d4na00364k

Herein, we demonstrate a novel approach for the fabrication of Cu_2O thin films grown on Ag nanowire (AgNW) networks for efficient electrocatalytic water oxidation. The AgNW networks can be easily deposited on the surface of copper substrates through a simple spray coating process,[27,28] followed by the atmospheric-pressure spatial atomic layer deposition (AP-SALD) of Cu_2O films having different thicknesses. Thus, the whole process takes place at atmospheric pressure and is compatible with high-throughput fabrication methods such as roll-to-roll.[29–32] The Cu_2O film structure, morphology, and properties have been previously optimized to produce conformal, pure, and homogeneous deposition.[33,34]

Electrochemical measurements showed that the obtained OER performance correlates with Cu_2O thickness, with the highest OER performance attained for Cu_2O coatings 50 nm thick: $\eta_{10} = 409$ mV and a Tafel slope of 47 mV dec^{-1}. To the best of our knowledge, these results are comparable and even surpass the performance of hitherto reported Cu-based OER electrocatalysts. This demonstrates that combining metallic nanowire networks with a thin oxide active layer is a promising strategy to enhance the performance and cost-efficiency of the water splitting process.

2. Experimental section

2.1. Deposition of AgNW networks

AgNWs dispersed in isopropanol were supplied by Protavic and synthesized by polyol process in the presence of poly(vinyl pyrrolidone) (PVP). The nanowire had a length and diameter of 8 μm and 80 nm, respectively. The AgNW suspension (23.6 g L^{-1}) was diluted down 100 times prior to deposition. AgNWs were deposited onto Cu substrates through a home-made pneumatic spray system with a N_2 flow at 3 bar and a flow rate of 5 drops every 20 seconds. Cu substrates were heated up to 110 °C during the spraying in order to facilitate the solvent evaporation. The desired resistance, *i.e.* the network density, was controlled by adjusting the number of spray cycles.

2.2. Deposition of Cu_2O coatings

The depositions were performed with a homemade AP-SALD system, as described in our previous works.[35] Cu(I)(hfac)(tmvs) (Epivalence, Limited) was used as Cu precursor, heated at 60 °C while the transport line between the bubbler and the manifold injection head was heated at 65 °C to avoid any condensation of the precursors within the lines. The substrate was heated at 220 °C during the depositions. A mass flow of 60 sccm was used for the precursor, which was diluted in an extra nitrogen flow of 60 sccm before being sent to the injection head. In addition, water was carried using a mass flow of 120 sccm, diluted with an extra 120 sccm N_2 flow with a nitrogen barrier of 120 sccm per outlet. The growth per SALD cycle was estimated as 0.35 ± 0.05 nm per cycle from ellipsometry analysis. The precursor and water were injected continuously from the manifold head onto the substrate that oscillated at a scanning speed of 10 cm s^{-1}. A copper substrate was used to grow the AgNW@Cu_2O nanocomposites.

2.3. Characterization techniques

The film structure was analyzed by X-ray diffraction using a SmartLab Rigaku diffractometer (Rigaku Corporation, Tokyo, Japan) in Bragg Brentano mode, equipped with a rotating anode of Cu K_α radiation operating at 45 kV and 200 mA. The surfaces morphology of the thin films was observed by scanning electron microscopy (SEM-FEG), GeminiSEM 300, equipped with a SDD (BRUKER AXS-30 mm^2) for EDS analysis. The pH measurement was performed with an InLab Versatile Pro pH electrode from Mettler Toledo. Ellipsometry was used to obtain the film thickness of Cu_2O coatings on glass substrate, using a compact Film Sense FS-1 ellipsometer.

2.4. Electrochemical measurements

The electrochemical measurements were conducted in a typical three-electrode configuration in a one-compartment electrochemical Teflon cell filled with 1 M KOH as electrolyte. The fabricated copper-based materials were used as the working electrode, while the reference electrode and counter electrode were an Ag/AgCl electrode and a Pt wire, respectively. The applied potential of the working electrode was controlled using a VersaSTAT 4 potentiostat. The potentials *vs.* the Ag/AgCl reference electrode were converted to the reversible hydrogen electrode (RHE) scale according to the equation:

$$E_{RHE} = E_{Ag/AgCl} + 0.059\ pH + E_{0Ag/AgCl}$$

where $E_{Ag/AgCl}$ is the measured potential against the reference electrode and $E_{0Ag/AgCl} = 0.197$ V at 25 °C. Linear sweep voltammetry (LSV) curves were acquired with a scan rate of 5 mV s^{-1}. Tafel slopes were derived from *iR*-corrected polarization curves by fitting experimental data to equation $\eta = a + b \log j$, where η is overpotential, a is Tafel constant, b is Tafel slope, and j is the current density.

The *iR* drop of the measurements was corrected for the solution resistance, which was determined using the electrochemical impedance spectroscopy (EIS) technique.[36] EIS measurements were conducted in potentiostatic mode with a frequency ranging from 100 kHz to 0.1 Hz, an AC voltage of 5 mV and under the potential corresponding to 1.65 V, where all tested electrodes underwent OER process.

3. Results and discussion

Fig. 1a depicts the spray-coating process for depositing AgNWs onto copper electrodes at a mild temperature (110 °C) to prevent substrate oxidation. Following AgNW spray deposition, the Cu_2O thin film is deposited by AP-SALD on top of the AgNWs to fabricate the nanocomposites (AgNWs@Cu_2O), as schematically shown in Fig. 1b. The specimen is static for the AgNW spray deposition while the airbrush is moving above the substrate; for the Cu_2O coating the AP-SALD head is static and the sample is moving. The use of such relative movements enables to obtain samples that are spatially homogeneous. Several samples were studied, namely, bare AgNWs on top of

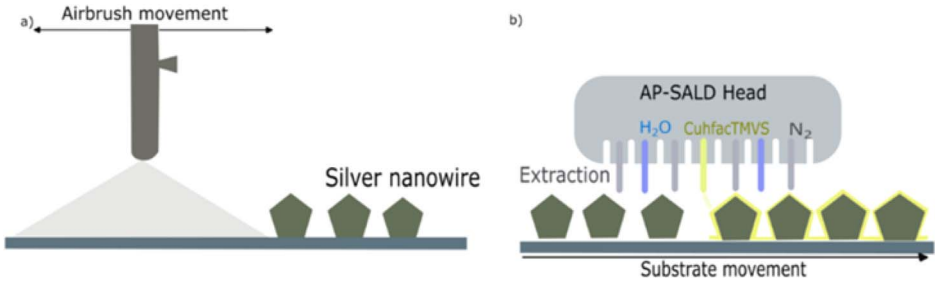

Fig. 1 Schematic illustration of the deposition process for (a) AgNW networks, and (b) Cu_2O thin films to fabricate AgNW@Cu_2O nanocomposite networks (note that this drawing is not to scale).

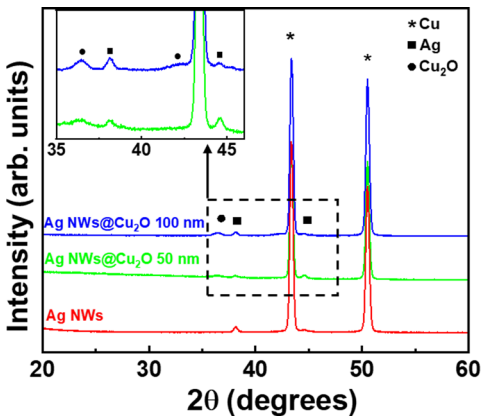

Fig. 2 Structural characterization by X-ray diffraction of various composite catalysts grown on Cu sheets.

a copper electrode, along with AgNW@Cu_2O composite electrodes having with different Cu_2O thicknesses.

The structure of the resulting catalysts was investigated using XRD (Fig. 2). The XRD diffraction pattern of bare AgNW networks on the Cu substrate reveals two main intense peaks at 2θ angles of 43.36° and 50.53°, corresponding to the (111) and (200) planes of the Cu substrate (JCPDS no. 04-0836). In addition, the pattern also shows two much less intense peaks at 38.1° and 44.56°, which correspond to metallic AgNWs (JCPDS no. 040783).[37] Finally, the patterns of composites with different oxide thickness, namely, AgNWs@50 nm-thick Cu_2O and AgNWs@100 nm-thick Cu_2O, show an additional weak peak at 36.45° which can be indexed to the (111) planes of Cu_2O (JCPDS No. 05-0667, reference XRD patterns for the SALD Cu_2O films can be found in our previous reports).[34] Furthermore, XPS studies performed on equivalent Cu_2O thin films showed only traces of Cu^+,[38,39] while silver will be observed as Ag 3d satellites.[40–42]

The morphology of as-deposited samples was assessed through SEM. Micrographs of AgNWs (Fig. 3a and d), show the typical morphology of AgNW networks. The nanowires homogeneously cover the surface of the copper sheet with a diameter of about 70 nm. The copper surface morphology beneath the AgNWs exhibits a rather rough texture with small pores. The surface morphologies of AgNWs@50 nm-thick and 100 nm-thick Cu_2O samples are shown in Fig. 3b, c, e, and f, respectively, where a thin layer of Cu_2O coats uniformly the surface of

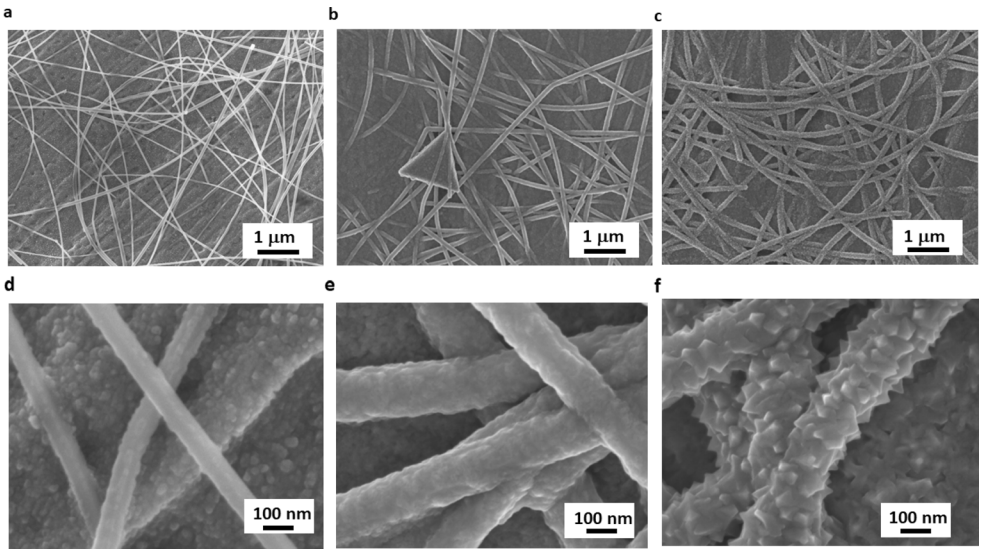

Fig. 3 Morphological analysis of various coatings deposited on Cu sheet. Low and high magnification SEM images of (a and d) bare AgNWs, (b and e) AgNWs@50 nm-thick Cu_2O, and (c and f) AgNWs@100 nm-thick Cu_2O.

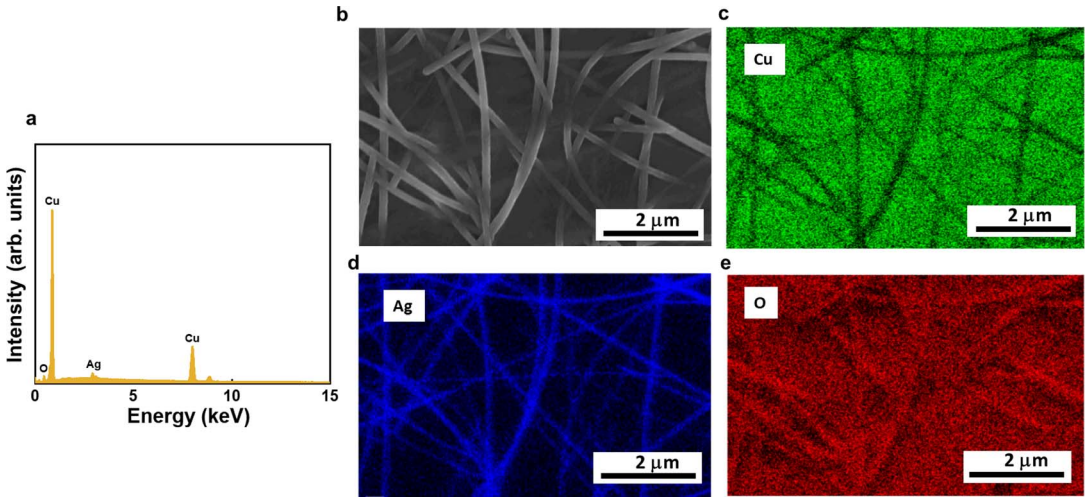

Fig. 4 (a) EDX spectrum of AgNWs/50 nm-thick Cu_2O. (b–e) SEM image and the corresponding elemental maps of AgNWs@50 nm-thick Cu_2O.

the AgNWs. Notably, the apparent diameter of AgNWs increases upon growing Cu_2O by AP-SALD leading to diameters of about ~100 nm. A lower Cu_2O film thickness results in a smoother layer with smaller grains, which tends to increase as the film thickness increases. This phenomenon was previously observed in our previous work involving the deposition of Cu_2O layer with different thicknesses on top of textured silicon heterojunctions.[35] Overall, the coating appears quite uniform and conformal, demonstrating the potential of using AP-SALD coating to achieve optimum conformality on the nanowires. Additionally, the composition of the various samples was assessed by means of EDX analysis. The EDX spectrum of AgNWs@50 nm-thick Cu_2O (Fig. 4a) shows as expected the presence of oxygen, silver, and copper peaks without any detectable impurity.

Furthermore, the elemental mapping, as determined by EDX (Fig. 4b–e), confirms that the Cu_2O coating is uniformly distributed along the AgNW backbone. Similar results were obtained for AgNWs/100 nm-thick Cu_2O (Fig. S1 and S2,† respectively).

To test the electrochemical performance of as-synthesized samples, a 3-electrodes configuration in 1 M KOH solution with a scan rate of 5 mV s^{-1} was employed. Initially, the OER electrocatalytic activities of bare Cu foil, AgNWs, AgNWs@50 nm-thick Cu_2O, and AgNWs@100 nm-thick Cu_2O were evaluated using the LSV technique. In polarization curves reported in Fig. 5a, the catalytic performance follows the following order: bare copper sheet < bare AgNWs < AgNWs@100 nm-thick Cu_2O < AgNWs@50 nm-thick Cu_2O. Specifically, bare AgNWs, AgNWs@50 nm-thick Cu_2O and AgNWs@100 nm-thick Cu_2O show an OER activity that by far outperforms that of bare Cu

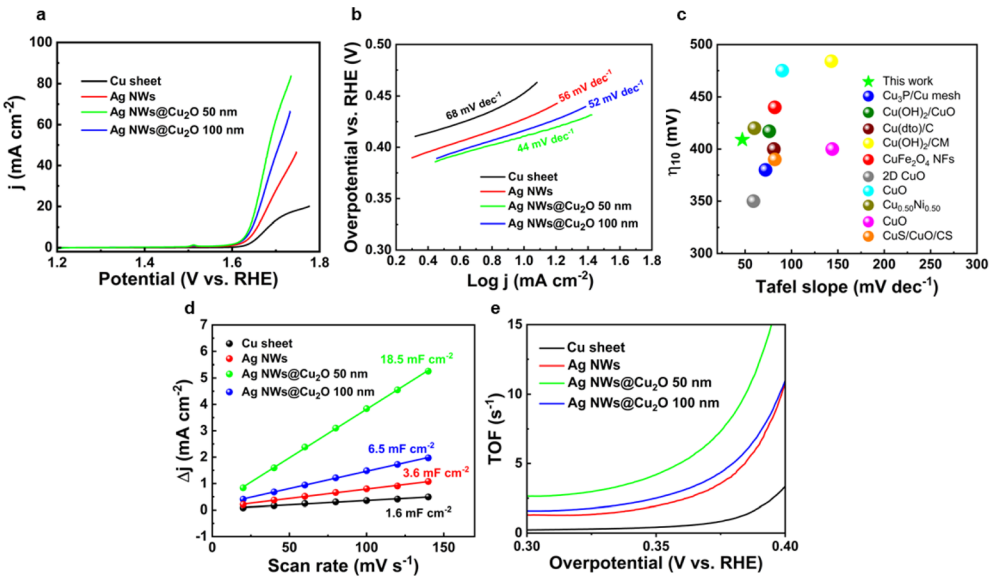

Fig. 5 OER performance of various coatings grown on Cu sheet in 1 M KOH. (a) Polarization curves, (b) corresponding Tafel plots, (c) comparison of η_{10} and Tafel slopes of some recent representative reports of copper-based OER catalysts, (d) current density plots, and (e) TOF plots.

Table 1 Comparison of previously reported Cu-based electrocatalysts for oxygen evolution reaction

Catalyst	Fabrication method	η_{10} (mV) *vs.* RHE	Tafel slope (mV dec^{-1})	TOF at 350 mV (s^{-1})	Electrolyte	Electrode	Duration of stability test (h)	Ref.
$Cu(OH)_2$/CuO	Galvanostatic anodization	417	76	—	0.1 M KOH	Copper foam	22	43
Cu(dto)/C	*In situ* electrochemical transformtion	400	81	—	1 M KOH	Glassy carbon electrode	—	44
$Cu(OH)_2$/CM	*In situ* chemical oxidation	484	143	—	1 M KOH	Copper mesh	16	45
$CuFe_2O_4$ NFs	Electrospinning	440	82	—	1 M KOH	Glassy carbon electrode	5.5	46
Cu_3P/Cu mesh	Phosphorization of Cu mesh	380	72	—	1 M KOH	Copper mesh	10	47
2D CuO	Chemical bath deposition	350	59	—	1 M KOH	Stainless steel	10	48
CuO	Chemical solution deposition method + annealing	475	90	—	1 M KOH	Fluorine doped tin oxide	10	49
$Cu_{0.5}Ni_{0.5}0$	Hydrothermal synthesis	420[a]	60	—	0.1 M KOH	Platinised silicon	4	50
CuO	Chemical solution method	400[b]	144	—	0.5 M KOH	Cu foam	6	51
CuS/CuO/CS	Solvothermal method	390	82		1 M KOH	Cu sheet	—	52
AgNWs@Cu_2O	AP-SALD (open atmosphere)	409	47	4.2	1 M KOH	Cu sheet	25	This work

[a] 1mA cm^{-2}. [b] 20 mA cm^{-2}.

substrate, with η_{10} of 427 mV, 409 mV, 416 mV, and 452 mV, respectively. The lowest value found for the thinner Cu_2O sample clearly suggests its superior catalytic behaviour. To investigate the catalytic kinetics of the two coatings, we evaluated the Tafel slopes extracted from LSV plots. A small Tafel slope usually suggests well-balanced kinetics throughout the water oxidation process.[53]

Fig. 5b shows the corresponding Tafel plots of the different catalysts. Tafel slopes of 68 mV dec^{-1}, 56 mV dec^{-1}, and 52 mV dec^{-1} were observed for Cu sheet, AgNWs, and AgNWs@Cu_2O 100 nm, respectively. Likewise, the lowest slope of AgNWs@50 nm-thick Cu_2O (44 mV dec^{-1}) suggests its augmented OER kinetics. The overpotential is largely dependent on the active surface area, and thus the enhanced results of the samples incorporating bare and coated AgNWs can be ascribed to the increased surface area. As far as the Tafel slope is concerned, it should be noted that it increases when large potential drops occur. The Ag nanowires could outperform as they realize a conductive highly porous backbone, leading to a low Tafel slope. Significantly, the η_{10} and Tafel slope of AgNWs@50 nm-thick Cu_2O is lower than most of the latest reported Cu-based electrocatalysts (see Fig. 5c and Table 1); the lower η_{10} needed to steer the OER reaction underscores the superior catalytic proficiency of the present catalyst, whilst the reduction in the Tafel gradient suggests a faster electron transfer capacity on the electrode surface. EIS was employed to probe the charge transport kinetics at the electrode/electrolyte interface. The Nyquist plots of all samples in 1.0 M KOH at a potential of 1.65Vvs. RHE are given in Fig. S3.† Charge transfer resistance follows the following order: bare Cu sheet < bare AgNWs < AgNWs@100 nm-thick Cu_2O < AgNWs@50 nm-thick Cu_2O. Overall, the AgNWs network morphology and thin Cu_2O layer serve the purpose of decreasing the charge transfer resistance and facilitate ionic diffusion, giving rise to the superior OER kinetics. Moreover, it is important to probe the possible reason behind the different electrocatalytic activity of the various

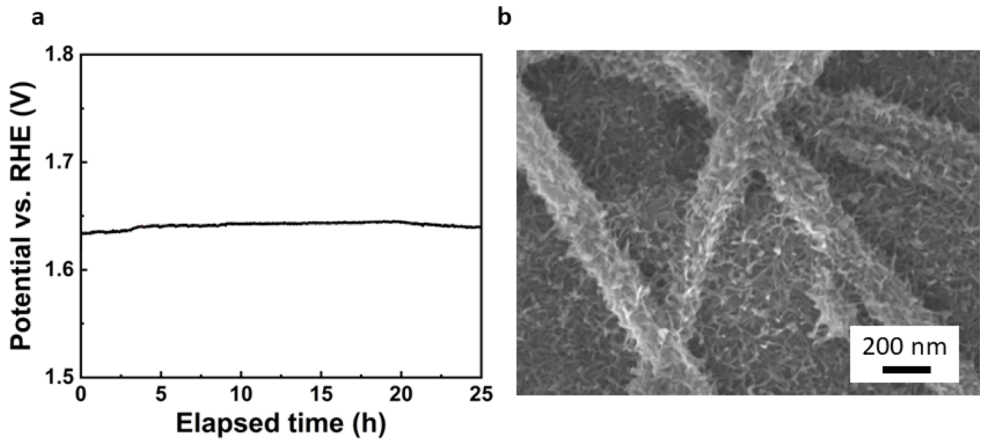

Fig. 6 (a) Chronopotentiometric curve and (b) SEM after OER of AgNWs@ 50 nm-thick Cu_2O.

samples. In this regard, Electrochemical Active Surface Area (ECSA) was evaluated by measuring the double-layer capacitance (C_{dl}) from the non-faradaic region of CV curves (further details are provided in ESI and in Fig. S4†).

As shown in Fig. 5d, the C_{dl} of the AgNWs@50 nm-thick Cu_2O (18.5 mF cm^{-2}) is much higher than that of AgNWs@100 nm-thick Cu_2O (6.5 mF cm^{-2}), AgNWs (3.6 mF cm^{-2}) and Cu sheet (1.6 mF cm^{-2}). The higher C_{dl} for the thickest sample is likely to be ascribed to its augmented surface area.[54,55]

The TOF parameter is crucial for assessing the OER performance because it is a hint of the intrinsic electrocatalytic activity of a catalyst. As presented in Fig. 5e, AgNWs@50 nm-thick Cu_2O presents higher TOF values at 350 mV of overpotential (4.2 s^{-1}) compared to those of AgNWs@100 nm-thick Cu_2O (2.4 s^{-1}), AgNWs (1.9 s^{-1}) and Cu sheet (0.4 s^{-1}), demonstrating its improved O_2 generation for each active site.

Based on an overall examination of the above electrochemical results, it can be inferred that the OER activity of the investigated catalysts is positively influenced by a reduction in thickness. As previously reported,[11,14] the reduced electrochemical performance for thicker samples can be ascribed to a higher potential drop occurring from the substrate to the top of the sample, which leaves a high portion of the film at a potential not sufficient to drive the electrochemical reaction.

Finally, the long-term stability of the most active catalyst was investigated through chronopotentiometric test. As illustrated in Fig. 6a, the voltage at a current density of 10 mA cm^{-2} shows only a slight increase upon 25 h of testing, demonstrating the stability of the electrode. SEM images of the sample after the chronopotentiometric test (Fig. 6b) reveal that the integrity of the composite is maintained. However, a change of morphology of the Cu_2O layer can be clearly observed. Such morphological evolution and its possible impact in the performance and stability of the catalyst needs to be further evaluated in future works.

From the above catalytic trend, we conclude that the AgNW network provides a significant increase in the catalytic activity compared to bare Cu substrate, which may be attributed to the following aspects: (1) enhanced electron transport owing to very high conductivity of Ag; (2) improved support-catalyst contact area, (3) excellent mass transfer for the escape of oxygen bubbles.[24,56]

Conclusions

In summary, we present the fabrication of Cu-based nanocatalysts aimed at enhancing the OER performance on the surface of AgNWs-coated copper substrates. Cu_2O thin films deposited on AgNWs providing a higher-dimensional network exhibited very good catalytic performance for electrocatalytic water oxidation. AgNWs@50 nm-thick Cu_2O grown on the surface of Cu sheet showed a lower η_{10} and Tafel slope compared to thicker catalyst and bare AgNWs. The enhanced catalytic efficiency can be attributed primarily to the significantly larger surface area and unique characteristics to furnish more active and accessible sites for catalysis. In addition, the electrodes presented here were fabricated by scalable, low-cost approaches. These results not only demonstrate the potential of nanostructured Cu-based electrode materials as low-cost, eco-friendly, and highly efficient electrocatalysts towards OER, but also trigger future research on this emerging class of electrode materials for water-splitting and other lectrochemical applications.

Data availability

The data supporting this article have been included as part of the ESI.†

Author contributions

S. Battiato: conceptualization, methodology, investigation, writing – original draft, writing, review & editing; A. Sekkat: investigation, conceptualization, visualization, methodology, writing – review & editing; C. S. Velasquez: investigation; A. L. Pellegrino: investigation; D. Bellet: methodology, conceptualization, writing, review & editing; A. Terrasi: project administration, funding acquisition, resources; S. Mirabella: conceptualization, methodology, writing, review & editing; D. Munoz-Rojas: resources, conceptualization, methodology, writing – review & editing.

Conflicts of interest

There are no conflicts of interest to declare.

Acknowledgements

This research was funded by the project AIM1804097 Programma Operativo Nazionale FSE – FESR "Ricerca e Innovazione 2014–2020", by the project "Programma di ricerca di ateneo UNICT 2020-22 linea 2 PIA.CE.RI", and by the project PNRR-MUR Samothrace (ECS_00000022). This work was partially supported by Bio-Nanotech Research and Innovation Tower grant BRIT PONa3_00136, University of Catania, for the structural characterization with SmartLab diffractometer facility. This work has been partially supported by the CDP Eco-SESA receiving funds from the French National Research Agency in the framework of the "Investments for the future" program (ANR-15-IDEX-02).

References

1 H. Zhou, F. Yu, Q. Zhu, J. Sun, F. Qin, L. Yu, J. Bao, Y. Yu, S. Chen and Z. Ren, *Energy Environ. Sci.*, 2018, **11**, 2858–2864.
2 Y. P. Zhu, C. Guo, Y. Zheng and S. Z. Qiao, *Acc. Chem. Res.*, 2017, **50**(4), 915–923.
3 I. Staffell, D. Scamman, A. V. Abad, P. Balcombe, P. E. Dodds, P. Ekins, N. Shah and K. R. Ward, *Energy Environ. Sci.*, 2019, **12**, 463–491.
4 Z. W. Seh, J. Kibsǵaard, C. F. Dickens, I. Chorkendorff, J. K. Nørskov and T. F. Jaramillo, *Science*, 2017, **335**, 146.

5 M. Tahir, L. Pan, F. Idrees, X. Zhang, L. Wang, J.-J. Zou and Z. L. Wang, *Nano Energy*, 2017, **37**, 136–157.
6 S. Divanis, T. Kutlusoy, I. M. Ingmer Boye, I. C. Manand and J. Rossmeisl, *Chem. Sci.*, 2020, **11**, 2943–2950.
7 Y. Yan, S. Liang, X. Wang, M. Zhang, S.-M. Hao, X. Cui, Z. Li and Z. Lin, *Proc. Natl. Acad. Sci. U. S. A.*, 2021, **118**, e2110036118.
8 Y. Yan, H. Cheng, Z. Qu, R. Yu, F. Liu, Q. Ma, S. Zhao, H. Hu, Y. Cheng, C. Yang, Z. Li, X. Wang, S. Hao, Y. Chen and M. Liu, *J. Mater. Chem. A*, 2021, **9**, 19489–19507.
9 X. Cui, L. Gao, S. Lei, S. Liang, J. Zhang, C. D. Sewell, W. Xue, Q. Liu, Z. Lin and Y. Yang, *Adv. Funct. Mater.*, 2021, **31**, 2009197.
10 X. Li, Y. Liu, H. Chen, M. Yang, D. Yang, H. Li and Z. Lin, *Nano Lett.*, 2021, **21**, 3098–3105.
11 S. Cosentino, M. Urso, G. Torrisi, S. Battiato, F. Priolo, A. Terrasi and S. Mirabella, *Adv. Mater.*, 2020, **1**, 1971.
12 L. Bruno, S. Battiato, M. Scuderi, F. Priolo, A. Terrasi and S. Mirabella, *Int. J. Hydrogen Energy*, 2022, **47**, 33988–33998.
13 S. Battiato, A. L. Pellegrino, A. Pollicino, A. Terrasi and S. Mirabella, *Int. J. Hydrogen Energy*, 2023, **48**(48), 18291–18300.
14 S. Battiato, M. Urso, S. Cosentino, A. L. Pellegrino, S. Mirabella and A. Terrasi, *Nanomaterials*, 2021, **11**, 3010.
15 S. Battiato, L. Bruno, A. L. P. A. Terrasi and S. Mirabella, *Catal. Today*, 2023, **423**, 1139239.
16 W. Zhang, Q. Jia, H. Liang, L. Cui, D. Wei and J. Liu, *Chem. Eng. J.*, 2020, **396**, 125315.
17 M. B. Gawande, A. Goswami, F. X. Felpi, T. Asefa, X. X. Huang, R. Silva, X. X. Zou, R. Zboril and R. S. Varma, *Chem. Rev.*, 2016, **116**, 3722–3811.
18 K. Kannimuthu, K. l Sangeetha, S. S. Sankar, A. Karmakar, R. Madhua and S. Kundu, *Inorg. Chem. Front.*, 2021, **8**, 234.
19 C.-C. Hou, W.-F. Fu and Y. Chen, *ChemSusChem*, 2016, **9**, 2069–2073.
20 J. Yu, Q. Cao, B. Feng, C. Li, J. Liu, J. K. Clark and J.-J. Delaunay, *Nano Res.*, 2018, **11**(8), 4323–4332.
21 C. C. L. McCrory, S. Jung, J. C. Peters and T. F. Jaramillo, *J. Am. Chem. Soc.*, 2013, **135**(45), 16977–16987.
22 Y. Li and S. Guo, *Nano Today*, 2019, **28**, 100774.
23 L. Bardet, D. T. Panastasiou, C. Crivello, M. Akbari, J. Resende, A. Sekkat, C. Sanchez-Velasquez, L. Rapenne, C. Jimenez, D. Munoz-Rojas, A. Denneuilin and D. Bellet, *Nanomaterials*, 2021, **11**, 2785.
24 H. Liu, S. Battiato, A. L. Pellegrino, P. Paoli, P. Rossi, C. Jimenez, G. Malandrino and D. Munoz-Rojas, *Dalton Trans.*, 2017, **46**, 10986.
25 Y. Sun, Y. Yin, B. T. Mayers, T. Herricks and Y. Xia, *Chem. Mater.*, 2002, **14**, 4736–4745.
26 X. Zhang, A. N. Marianov, Y. Jiang, C. Cazorla and D. Chu, *ACS Appl. Nano Mater.*, 2020, **3**, 887–895.
27 D. T. Papanastasiou, N. Charvin, J. Resende, V. H. Nguyen, A. Sekkat, D. Muñoz-Rojas, C. Jiménez, L. Flandin and D. Bellet, *Nanotechnology*, 2021, **32**(44), 445702.
28 D. T. Papanastasiou, A. Sekkat, V. H. Nguyen, C. Jiménez, D. Muñoz-Rojas, F. Bruckert and D. Bellet, *Adv. Mater. Technol.*, 2022, 2200563.
29 K. P. Mulsselman, C. F. Uzoma and M. S. Miller, *Chem. Mater.*, 2016, **28**(23), 8443–8452.
30 D. T. Papanastasiou, A. Schultheiss, D. Munoz-Rojas, C. Celle, A. Carella, J.-P. Simonato and D. Bellet, *Adv. Funct. Mater.*, 2020, 1910225.
31 D. Munoz-Rojas and J. Macmanus-Driscoll, *Mater. Horiz.*, 2014, **1**, 314–320.
32 A. Sekkat, D. T. Panastasiou, M. A. Ghani, H. Roussel, M. Weber, L. Rapenne, C. Jiménez, D. Muñoz-Rojas and D. Bellet, *Adv. Mater. Technol.*, 2023, 2301143.
33 A. Sekkat, M. O. Liedke, V. H. Nguyen, M. Butterling, F. Baiutti, J. De Dios, S. Veru, M. Weber, L. Rapenne, D. Bellet, G. Chichignoud, A. Kaminski-Cachopo, E. Hirschmann, A. Wagner and D. Muñoz-Rojas, *Nat. Commun.*, 2022, **131**(13), 1–11.
34 A. Sekkat, V. H. Nguyen, C. Arturo, M. D. La, L. Rapenne, D. Bellet, A. Kaminski-cachopo, G. Chichignoud and D. Muñoz-Rojas, *Commun. Mater.*, 2021, **2**, 78.
35 V. S. Nguyen, A. Sekkat, D. Bellet, G. Chichignoud, A. Kaminski-cachopo, D. Muñoz-Rojas and W. Favre, *J. Mater. Chem. A*, 2021, **9**, 15968–15974.
36 S. Battiato, L. Bruno, A. Terrasi and S. Mirabella, *ACS Appl. Energy Mater.*, 2022, **5**, 2391–2399.
37 L. Bardet, H. Roussel, S. Saroglia, M. Akbari, D. Muñoz-Rojas, C. Jimenez, A. Denneulin and D. Bellet, *Nanoscale*, 2024, **16**, 564–579.
38 A. Sekkat, M. Weber, J. López-Sánchez, H. Rabat, D. Hong, J. Rubio-Zuazo, D. Bellet, G. Chichignoud, A. Kaminski-Cachopo and D. Muñoz-Rojas, *Mater. Today Chem.*, 2023, **29**, 101431.
39 A. Sekkat, M. O. Liedke, V. H. Nguyen, M. Butterling, F. Baiutti, J. Sirvent, M. Weber, L. Rapenne, D. Bellet, G. Chichignoud, A. Kaminski-Cachopo, E. Hirschmann, A. Wagner and D. Muñoz-Rojas, *Nat. Commun.*, 2022, **13**, 5322.
40 Y. Wei, S. Chen, Y. Lin, X. Yuan and L. Liu, *J. Mater. Chem. C*, 2016, **4**, 935–943.
41 D. T. Papanastasiou, A. Mantoux, A. Crisci, H. Ribeiro, A. Sekkat, H. Roussel, M. Weber, L. Rapenne, C. Jiménez, M. Fivel, D. Bellet, E. Blanquet and D. Muñoz-Rojas, *ACS Appl. Nano Mater.*, 2024, **7**(11), 12312–12322.
42 D. C. Choo and T. W. Kim, *Sci. Rep.*, 2017, **7**, 1696.
43 N. Cheng, Y. Xue, Q. Liu, J. Tian, L. Zhang, A. M. Asiri and X. Sun, *Electrochim. Acta*, 2015, **163**, 102–106.
44 R. P. Putra, H. Horino and I. I. Rzeznicka, *Catalysts*, 2020, **10**, 233.
45 Y. Zuo, Y. Liu, J. Li, R. Du, X. Han, T. Zhang, J. Arbiol, N. J. Divins, J. Llorca, N. Guijarro, K. Sivula and A. Cabot, *Chem. Mater.*, 2019, **31**, 7732–7743.
46 M. Li, Y. Xiong, X. Liu, X. Bo, Y. Zhang, C. Han and L. Guo, *Nanoscale*, 2015, **7**(19), 8920–8930.
47 S. Wei, K. Qi, Z. Jin, J. Cao, W. Zheng, H. Chen and X. Cui, *ACS Omega*, 2016, **1**, 1367–1373.
48 S. M. Pawar, B. S. Pawar, B. Hou, J. Kim, A. T. A. Ahmed, H. S. Chavan, Y. Jo, S. Cho, A. I. Inamdar, J. L. Gunjakar, H. Kim, S. Cha and H. Im, *J. Mater. Chem. A*, 2017, **5**, 12747–12751.

49 A. Singh, T. Schneller, I. Valov, I. B. Singh, A. K. Srivastava and R. Waser, *J. Catal.*, 2020, **384**, 189–198.
50 S. Kumar, P.-H. Weng and Y.-P. Fu, *Mater. Today Chem.*, 2022, **26**, 101159.
51 X. Liu, S. Cui, M. Qian, Z. Sun and P. Du, *Chem. Commun.*, 2016, **52**, 5546.
52 L. Tabassum, M. K. Islam, I. P. Perera, M. Li, X. Huang, H. Tasnim and S. L. Suib, *ACS Appl. Energy Mater.*, 2022, **5**, 12039–12048.
53 Y. Yan, B. Wen, M. Liu, H. Lei, J. Yang, S. He, Z. Qu, W. Xia, H. Li and J. Zeng, *Adv. Funct. Mater.*, 2024, 2316100.
54 D. Lozano-Castellò, D. Cazorla-AmorÓs, A. Linares-Solano, S. Shiraishi, H. Kurihara and A. Oya, *Carbon*, 2003, **41**(9), 1765–1775.
55 S. Anantharaj, H. Sugime and S. Noda, *J. Electroanal. Chem.*, 2021, **903**, 115842.
56 H. Kang, Y. Kim, S. Cheon, G. R. Yi and J. H. Cho, *ACS Appl. Mater. Interfaces*, 2017, **9**(36), 30779–30785.